

Mobility Gradient of Polystyrene in Films Supported on Solid Substrates

Yoshihisa Fujii, Hiroshi Morita, Atsushi Takahara, and Keiji Tanaka

Abstract In this review, we show the distribution of glass transition temperature (T_g) in monodisperse polystyrene (PS) films coated on silicon oxide layers along the direction normal to the surface. Scanning force microscopy with a lateral force mode revealed that surface T_g (T_g^s) was lower than the corresponding bulk T_g (T_g^b). Interestingly, the glass transition dynamics at the surface was better expressed by an Arrhenius equation than by a Vogel–Fulcher–Tamman equation. Interdiffusion experiments for PS bilayers at various temperatures, above T_g^s and below T_g^b , enabled us to gain direct access to the mobility gradient in the surface region. T_g at the solid substrate was examined by fluorescence lifetime measurements using evanescent wave excitation. The interfacial T_g was higher than the corresponding T_g^b . The extent of the elevation was a function of the distance from the substrate and the interfacial energy. The T_g both at the surface and interface was also studied by the coarse-grained molecular dynamics simulation. The results were in good accordance with the experimental results. Finally, dynamic mechanical analysis for PS in thin and ultrathin films was made. The relaxation time for the segmental motion became broader towards the faster and slower sides, due probably to the surface and interfacial mobility.

Y. Fujii

Department of Applied Chemistry, Kyushu University, Fukuoka 819-0395, Japan

H. Morita

Soft Matter Modeling Group, Nanosystem Research Institute, National Institute of Advanced Industrial Science and Technology, Ibaraki 305-8568, Japan

A. Takahara

Institute for Materials Chemistry and Engineering, Kyushu University, Fukuoka 819-0395, Japan

K. Tanaka (✉)

Department of Applied Chemistry, Kyushu University, Fukuoka 819-0395, Japan

International Institute for Carbon-neutral Energy Research (WPI-I2CNER), Kyushu University, Fukuoka 819-0395, Japan

e-mail: k-tanaka@cstf.kyushu-u.ac.jp

Keywords Coarse-grained molecular dynamics simulation • Interface • Scanning force microscopy • Surface • Thermal molecular motion • Time- and space-resolved fluorescence spectroscopy

Contents

1	Introduction	2
2	Surface	4
	2.1 Two-Dimensional Modulus Mapping	4
	2.2 Glass Transition	5
	2.3 Mobility Gradient	9
	2.4 Molecular Dynamics Simulation	11
3	Substrate Interface	15
	3.1 Glass Transition	15
	3.2 Mobility Gradient	17
	3.3 Molecular Dynamics Simulation	19
4	Thin Films	21
	4.1 Supported Film	21
	4.2 Sandwiched Film	23
5	Conclusion	25
	References	26

1 Introduction

In the twenty-first century, materials have been strongly desired to be smaller and/or thinner for the construction of tiny devices. Such a trend is also the case for polymeric devices. Also, to design and construct highly functionalized memory devices, electron beam lithography has been applied to polymer materials. In this case, the linewidth is tremendously small, such as several tens of nanometer. Even in the traditional applications of coating, adhesion, lubrication, etc., polymer thin films are now being used [1]. In reality, it is not technically difficult to prepare such tiny polymeric pieces thanks to the advent of modern nanotechnology. However, once the polymer pieces become smaller than approximately 100 nm, their physical properties are altered from the corresponding bulk behaviors mainly due to “surface and interfacial effects” [2], leading to unexpected problems in products. Hence, to improve the functionality and stability of devices, the physical properties of tiny and thin polymer pieces must be precisely controlled after understanding the surface and interfacial effects.

In 1993, Reiter demonstrated anomalous dynamics of polystyrene (PS) in ultrathin films on the basis of de-wetting kinetics [3]. Ultrathin films started to break even at a temperature below the bulk glass transition temperature (T_g^b). Such a de-wetting behavior can be attained only by molecular motion on a relatively large scale. In addition, hole growth in the de-wet ultrathin films was much faster than that in thick films. These findings imply that the glass transition temperature (T_g) was lower for ultrathin films than for thick films. Then, in 1994, Keddie, Jones and

Cory, using ellipsometry, studied the temperature dependence of film thickness for PS films on Si etched with HF and found that T_g decreased with decreasing film thickness [4]. This study has prompted a number of additional studies [5–14]. As a result, it was found that the interaction between segments and solid substrate is one of the controlling factors for T_g of thin films. If an attractive interaction exists between them, the T_g of the thin films increases over that in the bulk because the substrate interface strongly restricts molecular motion in the films. Otherwise, the T_g is less than the bulk value, because of the presence of a surface layer in which molecular motion is more enhanced.

Forrest, Dutcher and coworkers have prepared free-standing PS films to study T_g in thin films [15, 16]. In this case, the film possesses two free surfaces instead of a combination of a free surface with the substrate interface. Their Brillouin light scattering measurements revealed that T_g for the free-standing thin films was lower than the T_g^b and that the extent of the difference was much more striking for the free-standing thin films than for those supported on the substrates. This result convincingly shows that the surface and interfacial effects are crucial factors that affect the thermal properties of ultrathin polymer films. However, the aforementioned studies tried to understand the average thermal behavior in the films.

There have also been studies on how the relaxation dynamics is distributed in the film along the direction normal to the surface. Dielectric relaxation spectroscopy enables us to gain access to the segmental dynamics in thin and ultrathin polymer films. Fukao and Miyamoto revealed that the distribution of relaxation times for the α process in PS thin films broadened with decreasing thickness, in addition to the T_g depression [17]. They discussed these experimental results in terms of a three-layer model with different mobilities: liquid-like, bulk-like, and dead layers. Torkelson and coworkers systematically studied the surface and interfacial effects on the T_g of thin and ultrathin polymer films by temperature-dependent fluorescence spectroscopy [18]. Inserting a layer containing fluorescent probes into a desired vertical position in the film, they succeeded in collecting information about T_g at various depths in the film. However, a clear variability of T_g at the interface with a substrate was not discerned in the depth region of 12 nm from the substrate. On the basis of inelastic neutron scattering measurements, Kanaya, Inoue and coworkers claimed the existence of the dead layer with the thickness of about 5 nm [19]. They also examined the relation of thickness to T_g for PS films on Si substrates with a native oxide layer [20]. When the film thickness went beyond approximately 10 nm, T_g was invariant even with decreasing thickness. This implies that in such an ultrathin region, the interfacial effect serves as a counterbalance to the surface effect. O’Connell and McKenna examined the creep compliance functions directly from the stress and strain data at a given temperature and thickness using a micro-bubble inflation method [21]. They rationalized their results taking into account the distribution of chain mobility normal to the surface.

In this review, we show our own results of thermal molecular motion of PS at the free surface by mainly scanning force microscopy and at the substrate interface by space-resolved fluorescence spectroscopy. To do so, we also adopt coarse-grained molecular dynamics simulation to strengthen experimental results. Finally, we

revisit the distribution of chain mobility along the direction normal to the surface by dynamic mechanical analysis. PS used in our experiments was synthesized by an anionic polymerization and thus its polydispersity index for all samples was lower than 1.1, or monodispersed.

2 Surface

2.1 Two-Dimensional Modulus Mapping

First of all, it is visually evident how thermal molecular motion at the surface in PS films is active in comparison with that in the internal bulk phase. To show this, modulus mapping at the surface was made as a function of temperature using scanning viscoelasticity microscopy (SVM) [22]. At first, a PS film with a number-average molecular weight (M_n) of 1×10^6 was in part scratched by a blade so that the silicon substrate was exposed to the air. Figure 1a shows a topographic image of the partly scratched PS film [23]. The height difference between the unscratched and valley regions was approximately 100 nm and was in good accord with the film thickness evaluated by ellipsometry. Hence, it is clear that the higher and lower regions in the image correspond to the PS and silicon wafer surfaces, respectively. Figure 1b shows two-dimensional mapping of surface modulus in the film at room temperature, which was simultaneously obtained with the topographic image [23]. Brighter and darker areas correspond to higher and lower modulus regions, respectively. Since the PS and silicon moduli at room temperature are 3 ~ 4 and 280 GPa, respectively, it is reasonable to claim that the PS surface was observed as the lower modulus region in the SVM image. To gain access to the absolute value of surface modulus by SVM, it is necessary to evaluate how a tip contacts with the surface [24]. This has been experimentally carried out at a given temperature. However, the temperature varies in this experiment, and this leads to technical difficulties in examining the temperature dependence of tip contact manner with the surface. Hence, the apparent surface modulus is here expressed in arbitrary unit.

Figure 2 shows the SVM images for the PS film collected at various temperatures from 200 to 400 K [23]. The surface modulus of the silicon substrate should be invariant with respect to temperature in the employed range, meaning that the contrast enhancement between the PS and Si surfaces with temperature reflects that the modulus of the PS surface starts to decrease. In the case of a lower temperature, the image contrast was trivial, as shown in the top row of Fig. 2. On the other hand, as the temperature went beyond 330 or 340 K, the contrast between the PS and Si surfaces became remarkable with increasing temperature. This makes it clear that the PS surface reached a glass–rubber transition state at around these temperatures. Here, it should be recalled that the T_g^b of the PS by differential scanning calorimetry (DSC) was 378 K. Therefore, it can be claimed that surface glass transition temperature (T_g^s) in the PS film is definitely lower than the corresponding T_g^b .

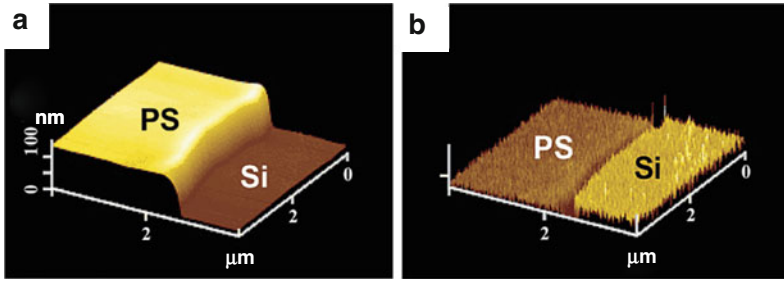


Fig. 1 PS film in part scratched by a blade: (a) surface morphology by AFM and (b) modulus mapping by SVM

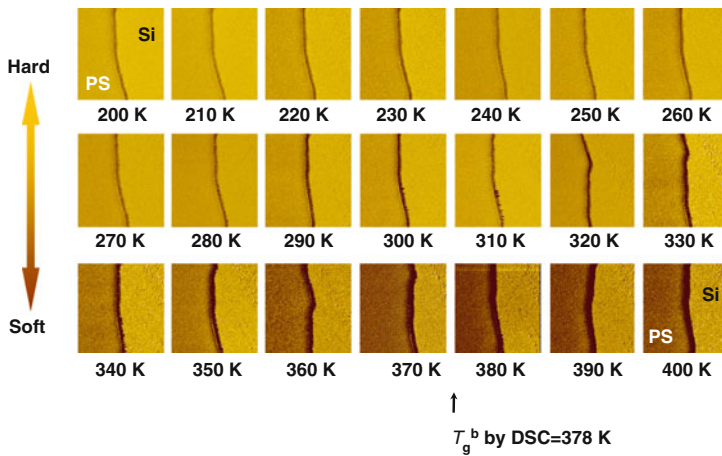


Fig. 2 SVM images of the film shown in Fig. 1 at various temperatures. The left- and right-hand side regions in each image correspond to PS and Si surfaces, respectively

2.2 Glass Transition

In this section, glass transition behavior at the surface in the PS films is discussed. Our experimental technique to probe this was lateral force microscopy (LFM) in addition to SVM. The details of why LFM can reveal such behavior are described elsewhere [24, 25]. In short, the central part of the idea is that lateral force, namely frictional force, is essentially related to energy dissipation. That is, lateral force is somehow proportional to loss modulus at the surface.

Figure 3 shows the lateral force versus temperature curves for the PS films with M_n of 4.9×10^3 (4.9k) and 140k at a fixed scanning rate (v) of $1 \mu\text{m s}^{-1}$ [26]. The thickness of the films was approximately 200 nm, which was sufficient to avoid the thinning effect on T_g [27]. The ordinate is normalized by the peak value of lateral

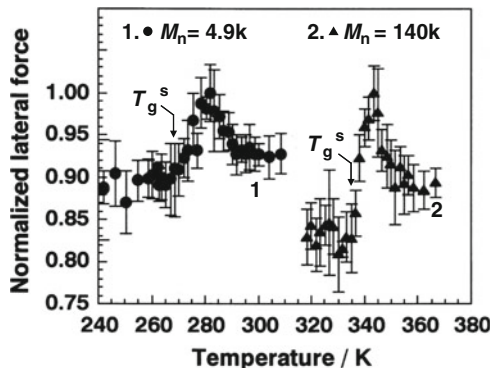


Fig. 3 Temperature dependence of lateral force curves at a given scanning rate. The curves for PS samples with M_n of 4.9k and 140k at the scanning rate of $1 \mu\text{m s}^{-1}$ are displayed. The T_g^b values measured by DSC were 348 and 376 K, respectively

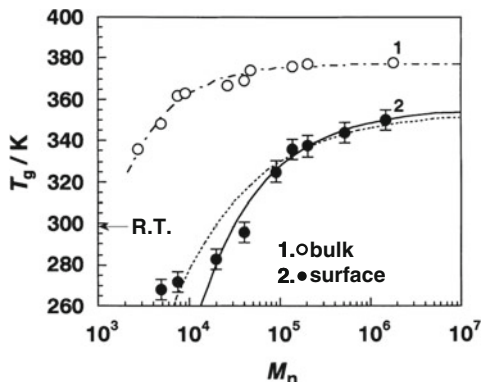


Fig. 4 Molecular weight dependences of T_g^b and T_g^s of the monodisperse PS, which were determined by DSC and LFM, respectively. The *arrow* beside the ordinate shows the room temperature. The *dotted curve 2* traces the T_g^s variations with M_n as deduced by Mayes' scaling theory. The *dashed curve 1* is drawn on the basis of the empirical equation established by Fox and Flory. The *solid curve* is drawn in the context of the power law analysis

force to show how the lateral force varies with temperature in the vicinity of a transition region. The lateral force-temperature curves shown in Fig. 3 reveal that each surface transition temperature for the PS films with M_n of 4.9k and 140k is much lower than their T_g^b of 348 and 376 K, respectively, as measured by DSC. This enhanced mobility at the surface has been in part explained in terms of the surface localization of chain end groups [24, 28–33], which might induce an extra free volume in the surface region. An onset temperature on the lateral force-temperature curve, that is, the temperature at which lateral force starts to increase, can be empirically defined as T_g^s .

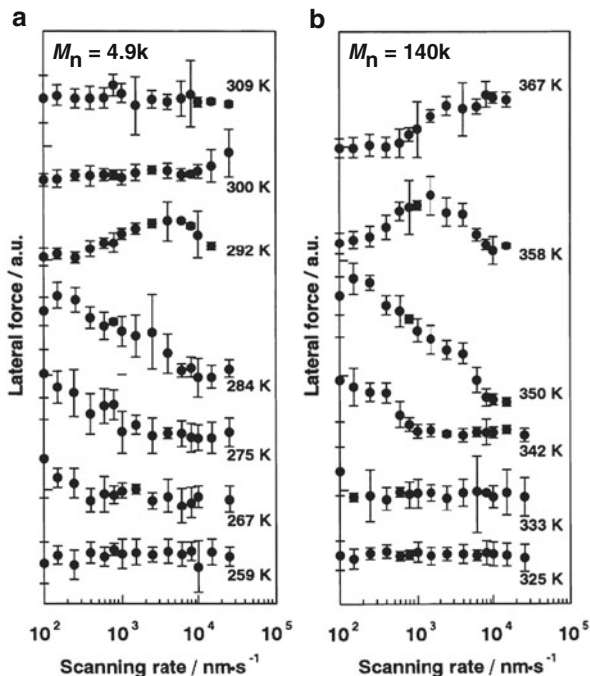
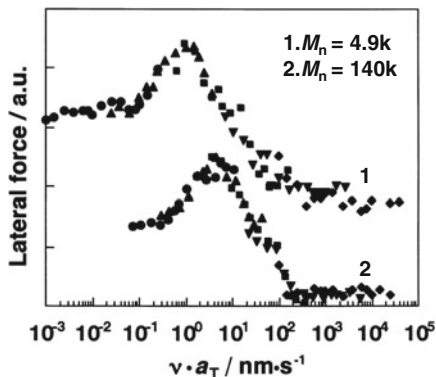


Fig. 5 Scanning rate dependence of the lateral force at various temperatures for the monodisperse PS films with M_n of (a) 4.9k and (b) 140k

Figure 4 shows T_g^s , obtained as a function of M_n , and T_g^b as determined by DSC [26]. The arrow beside the ordinate denotes our room temperature. T_g^s exhibited a stronger M_n dependence than T_g^b . Even at the ultrahigh M_n of 1,450k, at which the chain end effect should be ignored, the T_g^s was definitely lower than the T_g^b . The T_g^s value was dependent on chain end chemistry at a given M_n (not shown) [34]. The extent of the T_g depression at the surface was more striking for PS terminated with hydrophobic groups. Thus, although there is no doubt that the chain end segregation is one of factors determining the T_g depression at the surface, the effect cannot perfectly account for the enhanced mobility at the surface. Besides, the film surface was already in a glass–rubber transition or rubbery state at room temperature in the case of M_n smaller than approximately 40k. These results are in good accord with our parallel experiment using another technique, SVM [34].

Next, we will discuss whether the time–temperature superposition still holds at the surface. Figure 5 shows the relationships between scanning rate and lateral force on the PS films with M_n of 4.9k and 140k at different temperatures [26]. In both PS films, the lateral force was independent of the scanning rate at lower temperatures such as 259 and 325 K, as shown at the bottom of Fig. 5. It should be noted that the lateral force is invariant across two decades in the scanning rate if the surface is in a glassy state. Figure 5 shows that both surfaces with M_n values of 4.9k and 140k are

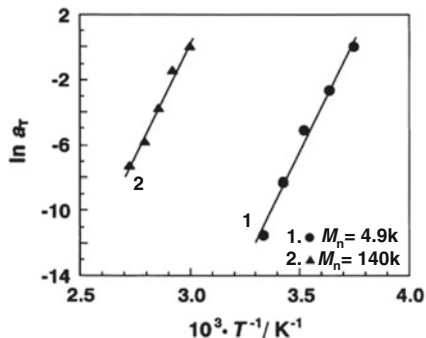
Fig. 6 Master curves of the scanning rate–lateral force relationship for the PS films with M_n of 4.9k and 140k drawn from the each curve in Fig. 5. Reference temperatures of 267 and 333 K were used for the PS films with M_n of 4.9k and 140k, respectively



in the glassy state up to about 259 and 325 K. These are in good accord with the results presented earlier that T_g^s with M_n values of 4.9k and 140k are 267 and 335 K, as shown in Fig. 4. When the measurement was carried out at higher temperatures, e.g., from 267 to 275 K and from 333 to 342 K for the PS films with M_n of 4.9k and 140k, respectively, the lateral force increased with decreasing scanning rate, especially at the lower scanning rates. Further, the lift-off point on the lateral force–scanning rate curve was shifted to the higher scanning rates. As the PS film was heated, a peak was clearly observed on the lateral force–scanning rate curve. The peak appeared in the temperature ranges of 284–292 K and 350–367 K for the samples of 4.9k and 140k, respectively. At temperatures higher than 300 and 367 K for the samples of 4.9k and 140k, the lateral force decreased with decreasing scanning rate. Eventually, the lateral force recovered the invariance with respect to the scanning rate, and this is shown at the top of Fig. 5a. Thus, the overall profiles reflect a successive change in the surface molecular motion from the glassy state to the rubbery state via the transition with increasing temperature. Because the performance of the piezoscanner was not stable at a temperature higher than 373 K, the LFM measurement for the PS with M_n of 140k was truncated at 367 K. The shape of each curve in Fig. 5 suggests that the master curves for the lateral force–scanning rate relation might be obtained by the horizontal and vertical shifts. Since the error bar was not necessarily small, only the horizontal shift (a_T) was quantitatively evaluated.

Figure 6 shows the master curves for the PS films with M_n of 4.9k and 140k drawn by horizontal and vertical shifts of each curve shown in Fig. 5 at the reference temperatures of 267 and 333 K, respectively [26]. The master curves obtained from the dependence of lateral force on the scanning rate were very similar to the lateral force–temperature curves, as shown in Fig. 3. Hence, it seems plausible as a general concept that the scanning rate dependence of the lateral force exhibits a peak in a glass–rubber transition. Also, it is clear that the time–temperature superposition principle, which is characteristic of bulk viscoelastic materials [35], can be applied to the surface relaxation process as well. Assuming that a_T has a functional form of Arrhenius type [36, 37], the apparent activation energy for the α_a -relaxation process, ΔH_a^\ddagger , is given by:

Fig. 7 Semilogarithmic plots of shift factor, a_T , versus reciprocal absolute temperature for the PS films with M_n of 4.9k and 140k



$$\ln a_T = \frac{\Delta H^\ddagger}{R} \left(\frac{1}{T} \right) \quad (1)$$

where R is the gas constant and T is the measurement temperature. Figure 7 shows the relationship between $\ln a_T$ and the reciprocal absolute temperature for the PS films with M_n of 4.9k and 140k, the so-called Arrhenius plots [26]. The activation energy for the surface α_a -relaxation process calculated from each slope in Fig. 7 was $230 \pm 10 \text{ kJ mol}^{-1}$, independent of M_n for the PS. This value was much smaller than reported values for bulk PS sample, which ranged from 360 to 880 kJ mol^{-1} [38, 39]. This implies that the cooperativity for the segmental motion at the surface was intensively reduced in comparison with that in the interior bulk region. Once this can be accepted, it is plausible that the thermal molecular motion at the PS surface was enhanced by not only the surface localization of chain end groups but also by the reduced cooperativity.

2.3 Mobility Gradient

So far, it has been clear that chain mobility at the surface is much more enhanced than that in the interior region. A question that should be addressed is how deep is the region in which the mobility is enhanced. The presence of a mobility gradient in the surface region of PS is discussed with reference to the results of interdiffusion experiments using bilayer films of PS and deuterated PS (dPS), which were prepared by attaching two original surfaces together, at various temperatures.

Figure 8 shows the time evolution of interfacial thickness for the PS/dPS bilayer as a function of temperature [40]. The M_n of both PS and dPS was fixed at 29k. The interfacial characterization was made by dynamic secondary ion mass spectroscopy (DSIMS). In the case of annealing at 400, 393, and 380 K (i.e., above the T_g^b of 376 K), the interfacial thickness proportionally increased to a half power of the annealing time. This is in good accordance with the context of Fickian diffusion. By contrast, a unique interfacial evolution was observed at 370 K (i.e., between T_g^s and T_g^b). At first, the bilayer interface monotonically thickened with increasing time,

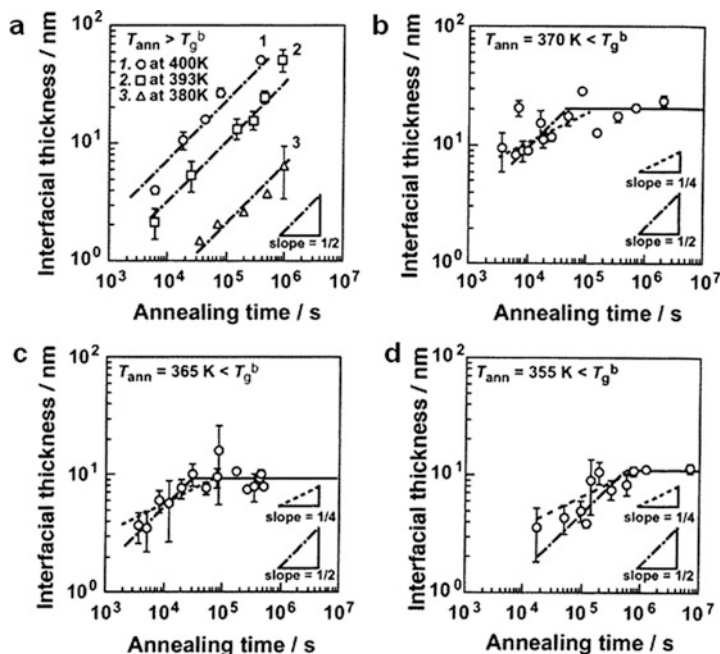


Fig. 8 Double-logarithmic plots of the relation between interfacial thickness and annealing time for hPS/dPS bilayer annealed at various temperatures: (a) 400, 393, and 380 K, i.e., above both T_g^b and T_g^s ; (b) 370 K; (c) 365 K; and (d) 355 K. In (b)–(d) the temperatures are below T_g^b and above T_g^s . The *dashed* and *dotted lines* are drawn in the context of Fickian and segmental diffusions, respectively

although the exponent of time could not be determined because of the data scattering. When the time proceeded to 10^5 s, however, the interfacial thickness remained constant at 20 ± 5.6 nm. Here, it should be noted that the bilayer interface was prepared by attaching two original surfaces of hydrogenated PS (hPS) and dPS together. Thus, the data mean that chains went across the “mobile” interface and then reached the “dead” bulk region in terms of diffusivity. In other words, half of the constant interfacial thickness evolved after a sufficiently long time would correspond to the surface layer, in which the mobility is enhanced in comparison with the internal bulk phase.

The annealing temperature dependence of such a surface mobile layer will now be discussed. At 370 K, the thickness of the surface mobile layer was 10 ± 2.8 nm. It should be of interest to compare the thickness with the chain dimension. Twice the radius of gyration ($2R_g$) of an unperturbed PS with M_n of 29k is calculated to be 9.3 nm. This value is comparable to the surface layer thickness. At 365 and 355 K, the interfacial thicknesses similarly increased with time at first and then became invariant with respect to the annealing time, as shown in Fig. 8c, d. The evolved interfacial thickness at 365 and 355 K were 9.6 ± 2.5 and 11.4 ± 0.9 nm, respectively. Half of these values, namely surface mobile layer thicknesses, are much

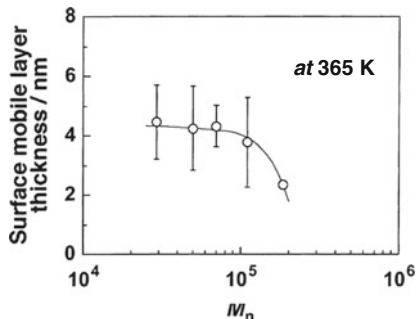


Fig. 9 Molecular weight dependence of surface layer thickness at 365 K

smaller than the unperturbed chain dimension, implying that segmental diffusion dominates the interfacial broadening of the PS/dPS bilayers at 365 and 355 K rather than center-of-mass diffusion.

Figure 9 shows the molecular weight dependence of surface mobile layer thickness at 365 K [40]. This temperature was well below T_g^b for all samples. Once it was confirmed that each bilayer interface was no longer evolving, the annealing treatment for the PS/dPS bilayers was stopped. The surface layer thickness was apparently insensitive to M_n up to 110k and then started to decrease with increasing M_n . Because the thickness was not scaled by $M_n^{1/2}$, it is clear that the thickness of the surface mobile layer is independent of the chain dimension; the thickness was not apparently related to the T_g difference between surface and bulk. Then, a question to clarified is why such a molecular weight dependence occurred as shown in Fig. 9. We again recall the chain end effect as a factor responsible for the enhanced surface mobility. Figure 10 illustrates a plausible cartoon of mobility gradients in the surface region [40]. At the depth range of a few nanometers from the surface, T_g should be strongly dependent on M_n because the concentration of segregated chain ends is dependent on M_n . Once the depth goes far beyond the segregation layer of chain ends, there is no reason why the mobility gradient in the surface region depends on M_n . This might be the reason for the results shown in Fig. 9.

2.4 Molecular Dynamics Simulation

On the basis of our results using scanning force microscopy such as SVM and LFM, we claim that the mobility at the surface of PS films is not the same as that in the bulk. However, in such measurements, a probe tip made of silicon or silicon nitride makes contact with the surface to be measured. This may induce some artifacts in the results. If an effect of tip contact on the surface dynamics cannot be negligible, our conclusion must be reconsidered. Thus, T_g^s is here discussed on the basis of coarse-grained molecular dynamics simulation using a bead-spring model of Grest

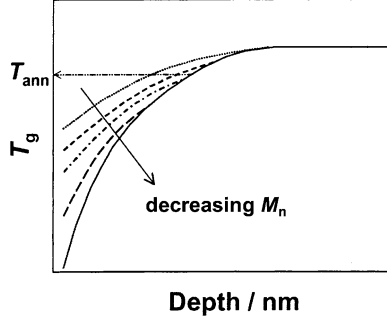


Fig. 10 Possible model for depth dependence of T_g as a function of M_n , showing the mobility gradient in the surface region. Within the depth region in which chain ends are segregated, the mobility gradient should be strongly dependent on M_n . This would be not the case far beyond the segregated surface layer of chain ends

and Kremer [41]. The polymer consists of N beads connected by the following potential $U^B(r)$:

$$U^B(r) = U^{\text{FENE}}(r) + U^{\text{LJ}}(r) \quad (2)$$

where r is the distance between the beads. $U^{\text{FENE}}(r)$ and $U^{\text{LJ}}(r)$ are given by:

$$U^{\text{FENE}}(r) = -(1/2)kR_0^2 \cdot \ln(1 - (r/R_0)^2), \quad (r \leq R) \quad (3)$$

$$U^{\text{FENE}}(r) = \infty, \quad (r < R) \quad (4)$$

$$U^{\text{LJ}}(r) = 4\epsilon \{[(\sigma/r)^{12} - (\sigma/r)^6] - [(\sigma/r^{\text{cut}})^{12} - (\sigma/r^{\text{cut}})^6]\}, \quad (\sigma \leq r^{\text{cut}}) \quad (5)$$

$$U^{\text{LJ}}(r) = 0, \quad (r > r^{\text{cut}}) \quad (6)$$

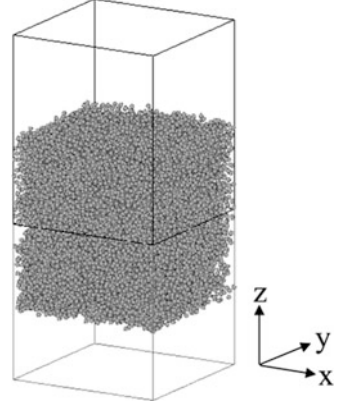
where k is the spring constant, R_0 is the maximum extension of the spring, ϵ is the unit of the energy, and σ is the unit of length. The nonbonding interaction between the polymer segments separated by the distance r is also given by the Lennard–Jones potential $U^{\text{LJ}}(r)$.

The time evolution of beads at position r_n is calculated by the Langevin equation as follows:

$$m(d^2r_n/dt^2) = -(\partial U/\partial r_n) - \Gamma(dr_n/dt) + \mathbf{W}_n(t) \quad (7)$$

where m is the mass of beads, U is the total potential energy of the system, Γ is the friction constant, and $\mathbf{W}_n(t)$ is a Gaussian white noise, which is generated according to the following equation:

Fig. 11 Model of polymer film used in the present work. The system consists of 100 chains each consisting of 100 beads. The size of the simulation box is $32\sigma \times 32\sigma \times 32\sigma$



$$\langle \mathbf{W}_n(t) \mathbf{W}_m(t') \rangle = 2k_B T m \Gamma \delta_{nm} I \delta(t - t') \quad (8)$$

We used the following parameter set: $k = 30.0\epsilon/\sigma^2$, $R_0 = 3.0\sigma$, $r^{\text{cut}} = 2.0\sigma$, and $\Gamma = 0.5\tau^{-1}$, where τ is the unit of time given by $\sigma(m/\epsilon)^{1/2}$. These parameters are the same as those of Grest and Kremer except for r^{cut} . The interval of one time step is 0.01τ . The unit of temperature is $T_0 = k_B/\epsilon$.

Figure 11 shows an example of the configuration for the simulation [42]. The figure shows the actual simulation box twice because the staggered reflective boundary condition is used: the chain in the bottom box is a mirror image of that in the top box with half-periodicity shifted. The thickness of the film is about 30σ , which is sufficiently larger than the root-mean-square of the polymer in the bulk region even for the largest polymer of $N = 200$. To study the segmental mobility near the surface, the film was divided into layers normal to the z axis and the mean-square displacement of the segment in each layer calculated in a time interval t . The thickness of the layer is σ , and a segment n is regarded to be in the layer l for the time interval between t' and $t' + t$ if the average z coordinate $[z_n(t') + z_n(t' + t)]/2$ is between σ_l and $\sigma_{(l+1)}$. The mean-square displacement of the segment in the layer l is defined as follows:

$$\varphi_l(t) = \frac{\sum_{t'} \sum_{n \text{ in layer } l} [r_n(t' + t) - r_n(t')]^2}{\sum_{t'} \sum_{n \text{ in layer } l} 1} \quad (9)$$

It must be mentioned that $\phi_l(t)$ becomes inappropriate for characterizing the surface mobility if t is taken to be very large: for large t , the diffusion of segments blurs the layer dependence of $\phi_l(t)$. For small t , however, $\phi_l(t)$ is a convenient quantity for characterizing the surface mobility.

Figure 12 shows $\phi_l(t^*)$ as a function of $z = \sigma l$ for various temperatures [42]. It is seen that the segmental mobility near the surface, $z = 13\sigma - 15\sigma$, differs

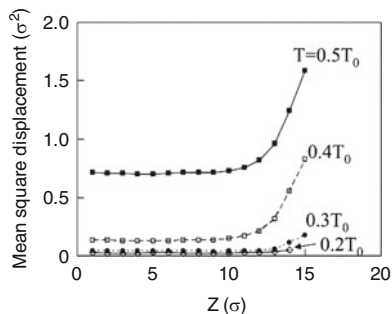


Fig. 12 Mean-square displacement of a polymer segment in a time interval t^* is plotted against the mean z position of the segment for various temperatures ($N = 100$). The average is taken for each layer of thickness 1σ

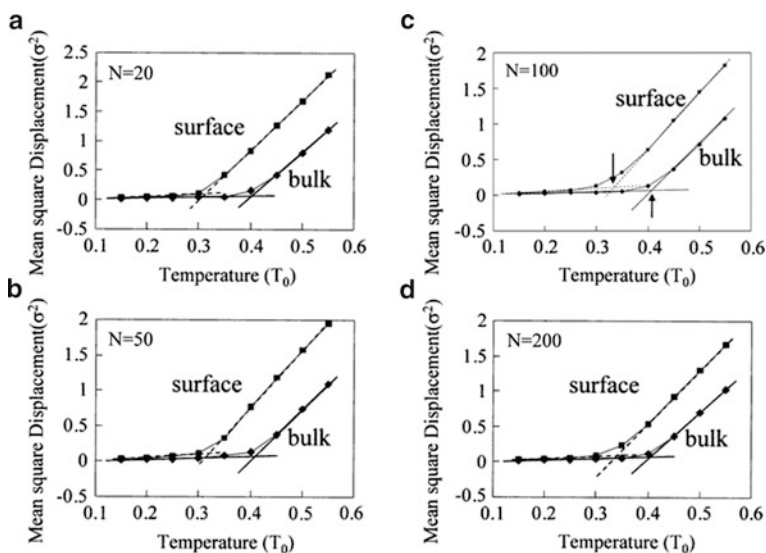
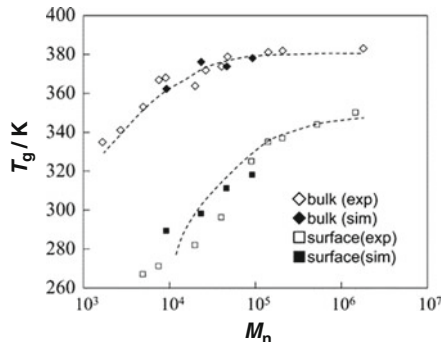


Fig. 13 Mean-square displacements of a polymer segment are plotted against the temperature for the case of $N = 20$ (a), 50 (b), 100 (c), and 200 (d)

significantly from that in the inner region, and that this surface region is limited to the thickness of about 3σ , which is about the same as that determined by the density profile. We will next describe analysis of the segmental mobility for the first three layers near the surface.

Figure 13 shows the mean-square displacement at the surface and in the bulk plotted against temperature for chains of $N = 20, 50, 100,$ and 200 [42]. It is seen that the mean-square displacement starts to increase sharply at a certain temperature, which can be associated with T_g . The characteristic temperature can be

Fig. 14 Glass transition temperatures are plotted against the molecular weight. *Filled symbols* indicate the results of molecular dynamics simulation, and *open symbols* indicate the results of the SFM experiment [26]



obtained by the intersection of the two lines characterizing the behavior at low and high temperatures. In all cases, the transition temperatures are clearly obtained.

Figure 14 shows the comparison between the experimental T_g^s by scanning force microscopy and that obtained by this simulation [42]. The agreement between the experiment and simulation looks to be very good. This indicates that the change of the T_g near the surface is well represented by the simulation. That is, it can be claimed that the effect of tip contact on T_g^s is trivial, if any. In conclusion, the chain mobility in the surface region is enhanced in comparison with that in the interior region, and the extent of the enhancement becomes more significant with proximity to the outermost surface.

3 Substrate Interface

3.1 Glass Transition

In this section, thermal molecular motion at the interface with solid substrates is discussed. It is needless to say that the issue is of pivotal importance for inherent scientific interest because motion at the interface seems to be totally different from that at the polymer surface. Also, the interface between polymers and inorganic materials is crucial in designing and constructing highly functionalized nanocomposites [43–45], which are now used for biomaterials [46, 47], sensors [48, 49], power sources [50, 51], etc., in addition to their popular and traditional use as structural materials [43–45, 52, 53].

We have developed a direct and noninvasive method to determine T_g of polymers at the interface with solid substrates [54, 55]. The strategy is to use fluorescence lifetime measurements using evanescent wave excitation. Figure 15a shows PS-NBD, i.e., PS containing the dye 6-[N-(7-nitrobenz-2-oxa-1,3-diazol-4-yl)amino]hexanoic acid (NBD) [55]. The NBD fraction of PS was sufficiently low to avoid self-quenching of the dye. The NBD dye was excited with the second-harmonic generation of a mode-locked titanium:sapphire laser equipped with a

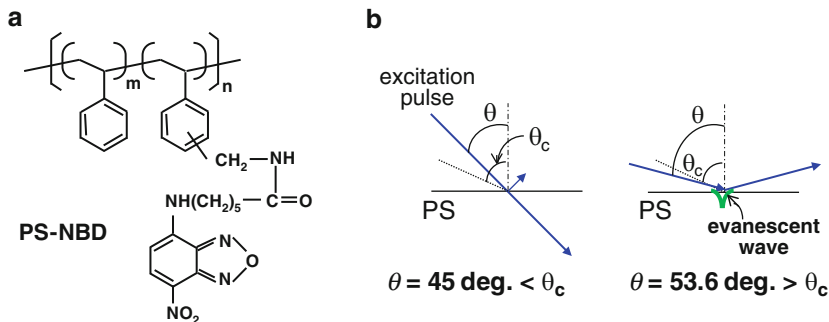


Fig. 15 (a) Chemical structure for PS-NBD. (b) Scheme for the measurement at $\theta = 45^\circ$ and 53.6° , being respectively smaller and larger than the critical angle of θ_c

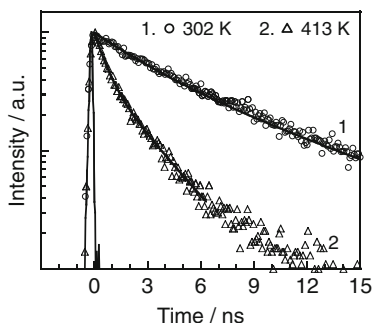


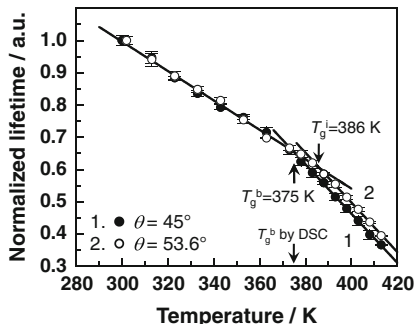
Fig. 16 Fluorescence decay curves from NBD tagged to PS with M_n of 53.4k in a film at 302 and 413 K

pulse selector and a harmonic generator. A streakscope was used to detect the time-resolved fluorescence from excited NBD molecules. Figure 15b shows the principle of the measurement. An excitation pulse was irradiated on the film from the substrate side via a prism at various incident angles. When the incident angle (θ) is larger than the critical angle (θ_c), the excitation pulse is totally reflected at the interface between the PS and the substrate. In this case, an evanescent wave, where the electric field exponentially decays along the direction normal to the interface, is generated at the PS interface. Information near the substrate interface was extracted on the basis of this evanescent wave excitation.

Figure 16 shows the time (t) dependence of the fluorescence intensity (I) from a PS film labeled with NBD dyes observed at 302 and 413 K [55]. The decay curves were fitted by the following double-exponential equation with two time constants, τ_{fast} and τ_{slow} :

$$I = I_0 \{ (1 - x) \exp(-t/\tau_{\text{fast}}) + x \exp(-t/\tau_{\text{slow}}) \} \quad (10)$$

Fig. 17 Temperature dependence of the lifetime for NBD tagged to PS with M_n of 53.4k in a film. Lifetimes are normalized by the value obtained at room temperature



where I_0 and x are the fluorescence intensity right after the excitation and the fraction of the slow component, respectively. While τ_{slow} was 7.45 ± 0.11 ns at 302 K, it decreased to 2.69 ± 0.01 ns at 413 K. This is simply because the fractional amount of non-radiative pathways to the ground state for excited species increased with temperature.

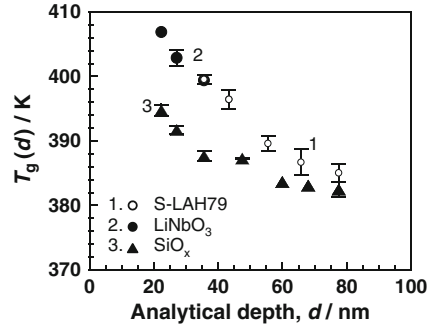
Next, lifetime measurements for NBD tagged to PS with M_n of 53.4k in the film on the S-LAH79 substrate, which was a glass with a higher refractive index, were made as a function of temperature. The θ_c value for this system can be simply calculated to be 51.3° by Snell's law. Figure 17 shows the temperature dependence of the fluorescence decay time constants at $\theta = 45^\circ$ and 53.6° [55]. In the case of $\theta = 45^\circ$, the excitation pulse went through the internal bulk phase of the film, meaning that the data reflect bulk information. The lifetime decreased with increasing temperature, and the slope was changed at 375 K, as shown by the filled circles in Fig. 17. As the measurement temperature increases beyond the temperature at which molecular motion releases, the slope of the temperature–lifetime relation should change because the dynamic environment surrounding the dye molecules changes at that temperature [18, 54]. Actually, the inflection point related to the slope change coincided with the T_g^b for the matrix PS of 375 K found by DSC. Thus, it is reasonable to claim that the fluorescence lifetime measurement using NBD probes tagged to a polymer allows us to determine the T_g of the matrix polymer.

When the θ value was higher than θ_c , the incident pulse was totally reflected at the interface between the PS and S-LAH79 substrate. That is, the NBD dye molecules near the interface were selectively excited by the evanescent wave. Hence, the data set obtained at $\theta = 53.6^\circ$ reflects the interfacial molecular motion. The inflection temperature, which can be assigned to the interfacial T_g (T_g^i) at $\theta = 53.6^\circ$, was 386 K, and was discernibly higher than the T_g^b . This is direct evidence for depressed mobility at the interface.

3.2 Mobility Gradient

The analytical depth of the above-mentioned technique is discussed in this section. The penetration depth (d_p) of the evanescent wave is given by [56]:

Fig. 18 Analytical depth dependence of T_g for PS with M_n of 53.4k at interfaces with various substrates



$$d_p = \lambda_0(\sin^2 \theta - \sin^2 \theta_c)^{-1/2} / 2\pi n \quad (11)$$

where λ_0 is the wavelength of the excitation light. In fact, the relation between the depth and the electric field intensity (I_{ev}) is much more important for the interfacial selectivity than the d_p value [56]:

$$I_{ev} = I_{ev,0} \exp(-2\zeta/d_p) \quad (12)$$

Here, ζ is the depth from the interface. The analytical depth (d) is defined as the position at which I_{ev} becomes $I_{ev,0}/e$, namely, the value of I_{ev} corresponding to $(d_p/2)$. The minimum d value attained in our experiment was 22.4 nm for the interface between LiNbO₃, which was also a material with a higher refractive index, and PS at $\theta = 74^\circ$. This value appears to be larger than the depth range in which the mobility gradient exists. However, taking into account the fact that the electric field intensity of the evanescent light is the strongest at the interface and exponentially decays with increasing depth, it is likely that the results obtained by the method proposed in this study mostly reflect the chain mobility near the interface with the solid substrate.

Equations show that the d value can be regulated by changing the angle θ of the excitation pulse and/or the refractive index n of the inorganic substrate. The d value decreases with increasing θ . In addition, two different substrates were used: an optical glass (S-LAH79) with an n of 2.05 and LiNbO₃ with an n of 2.30. To attain a smaller d value, the n value should be larger. However, it must be kept in mind that an alteration of the substrate causes a change in the interaction between PS and substrate. Figure 18 shows the relation between the analytical depth and T_g for PS with M_n of 53.4k on S-LAH79 and LiNbO₃. As a general trend, the T_g value increased with decreasing analytical depth. Interestingly, the curves for PS on S-LAH79 and LiNbO₃ are superimposed. To investigate this, the surface free energy for both substrates was examined by contact angle measurement with water and diiodomethane as probe liquids [57]. The numbers so obtained for S-LAH79 and LiNbO₃ were 38.1 and 38.3 mJ m⁻². These values can be regarded as the same within the experimental accuracy. Thus, it seems most likely that the surfaces of S-LAH79 and LiNbO₃ are chemically the same, probably due to the

antireflective surface coating, and hence the interaction between PS and the substrate is the same in the two cases.

According to Maxwell's equation for electromagnetic waves [58, 59], the analytical depth d is not changed even when the surface of a medium with a higher refractive index is coated with a layer, provided that the thickness of the layer is less than the analytical depth. On the other hand, the chemical interaction between a polymer and the substrate should be strongly altered due to the presence of the layer. Accordingly, both S-LAH79 and LiNbO₃ coated with a thin SiO_x layer with a thickness of at most 10 nm were used as substrates. Here, the combination of PS with SiO_x is regarded as a model system for a PS film on a silicon wafer. In this case, the d value was controlled by the refractive indices of PS and the substrate in addition to the incident angle of the excitation pulse. The T_g value for PS on S-LAH79 and LiNbO₃ coated with a thin SiO_x layer increased with decreasing analytical depth, as marked by the filled triangles in Fig. 18. Although the variation was similar for both S-LAH79 and LiNbO₃ substrates, marked by open and filled circles in Fig. 18, the extent was clearly depressed. The surface free energy of S-LAH79 and LiNbO₃ was approximately 38 mJ m⁻², comparable to that of PS, 40.6 mJ m⁻². On the other hand, the value for the SiO_x layer was measured to be 61.2 mJ m⁻², indicating an unfavorable interaction between PS and SiO_x. This may cause a reduction in the amount of restriction of segmental motion at that interface. Then, a question that arises is why T_g must increase at the substrate interface without an attractive interaction. For the moment, we suggest that the interface, which can be regarded as a hard wall, acts as an obstacle to the movement of polymer chains. As far the chain mobility at the outer most interface, we also studied the chain conformation of the PS, at a quartz substrate interface by sum-frequency generation (SFG) spectroscopy [60]. The chain conformation at the interface with the neutral substrate was not altered even at temperatures in excess of the corresponding bulk T_g . This also implies that polymer chains at the substrate interface are not much relaxed under the usual annealing condition determined from the polymer dynamics in the bulk.

3.3 *Molecular Dynamics Simulation*

The space- and time-resolved fluorescence spectroscopy clearly revealed that there exists a mobility gradient proximal to the substrate interface. However, it was not possible to gain access to mobility information in the depth shallower than 20 nm by this method. This again motivated us to estimate T_g as a function of the distance from the interface on the basis of coarse-grained molecular dynamics simulation (details are given in Sect. 2.4). Figure 19 shows the mean-square displacement at surface, bulk, and interface plotted against temperature for 170 chains [55]. One chain consists of 100 segments, which is larger than the critical number of segments that will initiate entanglements (i.e., 35). The mean-

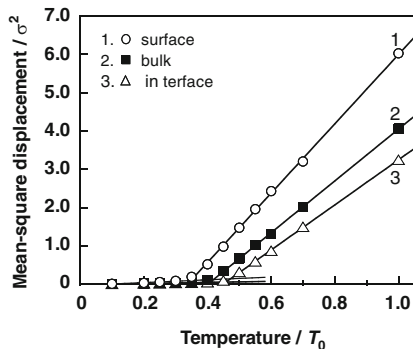


Fig. 19 Temperature dependence of mean-square displacement in three regions: surface, bulk, and interface. The data in each region (surface, bulk, and interface) is averaged over values in three layers of the simulation model, or 3σ

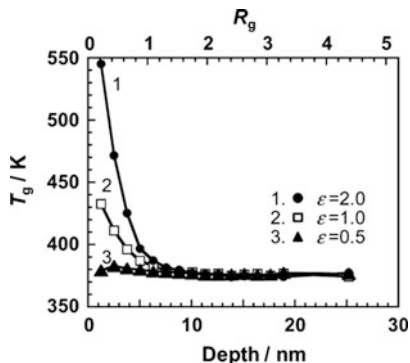
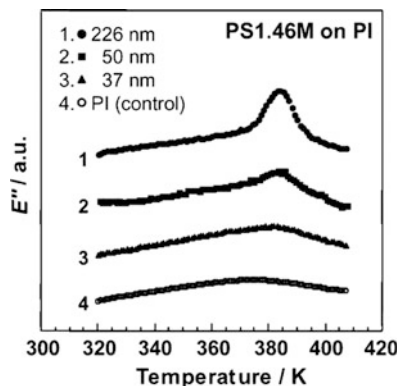


Fig. 20 Depth dependence of T_g for PS obtained by coarse-grained molecular dynamics simulation. The 0 depth is at the substrate interface, and the value is in a real space. The *upper abscissa* is expressed by the chain dimension using radius of gyration (R_g) for an unperturbed polymer chain. The ϵ value corresponds to Lennard–Jones energy between segments and substrate wall

square displacement started to increase sharply at a threshold temperature here defined as T_g , which was obtained from the intersection of the two lines characterizing the behavior at low and high temperatures. The T_g values at the surface, in the bulk, and at the substrate interface were claimed to be $0.35T_0$, $0.41T_0$, and $0.46T_0$, respectively.

Figure 20 shows the relation of T_g to depth from the interface. The T_g increased closer to the interface [55]. This trend became striking with increasing interaction between segments and substrate, namely, with an increase in the parameter ϵ . Interestingly, the depth region in which T_g was elevated was on the order of the radius of gyration of an unperturbed chain. On the other hand, in the case of the smallest ϵ ($\epsilon = 0.5$), a clear elevation of T_g at the substrate interface was not

Fig. 21 Temperature dependence of the loss modulus E'' for PS1.46M thin and ultrathin films coated on PI substrates. The data for a control PI are also shown



observed. These results indicate the extent to which T_g increases at the substrate interface is strongly dependent on the surface free energy of the substrate, and are in good accord with the experimental results.

4 Thin Films

4.1 Supported Film

Finally, dynamic mechanical analysis (DMA) for PS in thin and ultrathin films is discussed. Studies over the past 15 years have shown that the T_g of nanometer thick polymer films can vary significantly with the film thickness (h) when h falls below 50 nm [61–65]. Although the T_g has been found to both increase [5, 66, 67] and decrease [4, 10, 63, 68, 69] with decreasing h , the latter has drawn vastly more attention because of the significantly bigger size of the effect.

A Rheovibron DDV-01FP (A&D, Tokyo, Japan) tester has been used for DMA. In general, DMA has been accepted as a powerful method for studying the relaxation behavior of bulk samples. However, previous to these experiments, no one knew whether the technique was sensitive enough to be used with thin and ultrathin polymer films. To answer this question, a dynamic viscoelastic measurement for thin PS films supported on substrates was conducted.

Figure 21 shows the temperature dependence of the loss modulus (E'') for PS films of various thicknesses on polyimide (PI), together with the data for a control PI substrate. For reasons of space, only the data at the frequency of 11 Hz are presented. In the case of the 226 nm film, an α_a absorption peak corresponding to the segmental motion was observed on the temperature– E'' curve at around 380 K. The peak temperature was dependent on the frequency (not shown), meaning that the peak was assignable to not artifacts but to a relaxation process. This result is in good accordance with the corresponding bulk data.

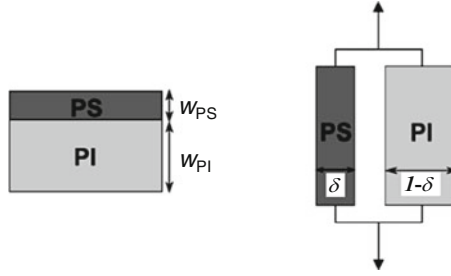


Fig. 22 Schematic representation of Takayanagi’s parallel model for PS on PI. See text for details

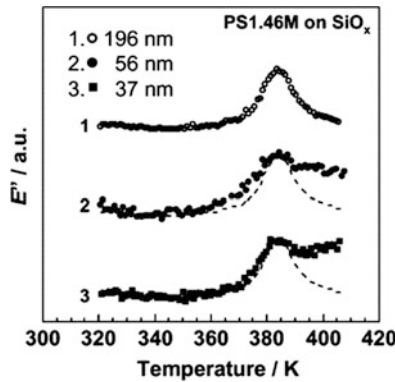


Fig. 23 Temperature dependence of E'' for PS1.46M thin and ultrathin films on SiO_x substrates

Because the volume ratio of the PS phase to that of the total system, the intensity of the α_a relaxation peak for the PS decreased as the films became thinner. However, a mechanical model analysis was able to be applied to the raw data to extract the contribution from the PS phase.

Figure 22 illustrates Takayanagi’s parallel model, in which the dynamic strain is everywhere constant [70]. Here, w is the film thickness in nanometers and δ is the volume fraction of PS. On the basis of this model, E'' can be formulated for a PS film coated on PI (E''_{all}) by:

$$E''_{\text{PS}} = \{(w_{\text{PI}} + w_{\text{PS}})E''_{\text{all}} - w_{\text{PI}}E''_{\text{PI}}\} / w_{\text{PS}} \quad (13)$$

Figure 23 shows the temperature dependence of background-subtracted E'' as a function of thickness for PS films of $1.46 \times 10^6 M_n$ (PS1.46M) on the SiO_x substrate. The values of E'' for the ultrathin films were again arbitrarily rescaled to have the same peak height as that for the 200 nm thick films. The α_a absorption peak was clearly observed, even for the ultrathin films with thicknesses of 56 and 37 nm. The temperature absorption curve for the 196 nm film on the SiO_x was in good

accordance with that for the 226 nm film on the PI, a result suggesting that the interfacial effect on the α_a relaxation process is negligible in this thickness region. More precisely, even if the surface and interfacial effects on molecular motion exist, they are not detectable for this thickness range. On the other hand, for the thinner films, the shape of the α_a absorption peak depended on which substrate was used. An obvious difference was observed between the ultrathin films on the SiO_x and PI substrates on the higher temperature side of the peak. For the ultrathin films on the PI, E'' monotonically decreased with increasing temperature, as shown in Fig. 21. In contrast, in the case of the ultrathin films on the SiO_x substrates, E'' slightly decreased, and then remained almost constant, or increased again after the peak, as shown in Fig. 23. This result implies that the fractional amount of slower relaxation times in the ultrathin films on the SiO_x is larger than that in the corresponding films on the PI. Thus, it seems most likely that the chains that are in contact with the SiO_x layer are less mobile than those next to the PI. For the ultrathin films on the PI, the peak broadening on the lower temperature side became more marked with decreasing thickness. Postulating that the surface segmental motion might be more detectable with decreasing thickness due to the larger surface-to-volume ratio, this result seems reasonable. However, we observed a unique thickness dependence of the broadening for the ultrathin films on the SiO_x . In the case of the 56 nm thick film, we noted the peak broadening on the lower temperature side, but on the other hand, we did not observe it for the thinner, 37 nm thick film. These findings may indicate that the molecular motion in the surface region is inhibited by a restriction from the interface, if the interfacial effect is strong.

4.2 Sandwiched Film

According to the above-mentioned results, it is expected that the restriction from the interface should be striking for the ultrathin PS films sandwiched between the SiO_x layers. Therefore, the segmental motion in PS films sandwiched between SiO_x layers, in which the top layer was prepared by a vacuum-deposition procedure, is discussed next.

Figure 24 shows the temperature dependence of background-subtracted E'' as a function of thickness for the PS1.46M films between the SiO_x layers. Even in the case of the 211 nm film, an additional shoulder on the higher temperature side of the α_a relaxation peak was observed. As the film thinned, the high-temperature shoulder evolved and eventually became a clear peak. Since the presence of the additional peak for the 37 nm film sandwiched between the SiO_x layers depended on the frequency employed, it is clear that the peak derived from a relaxation process. In addition, in the case of the sandwiched films, the relaxation peak did not broaden on the lower temperature side, even though the films became thinner. This result can be easily understood by taking into account the film geometry. In other words, the free surface disappeared under the capping SiO_x layer, and the interfacial region with the SiO_x layer doubled. On the basis of the results mentioned above, we suggest that

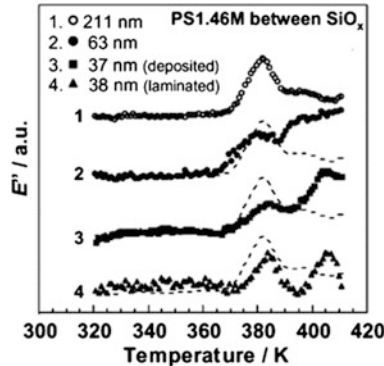


Fig. 24 Temperature dependence of E'' for PS1.46M thin and ultrathin films sandwiched between SiO_x layers

the main and additional peaks observed at the lower and higher temperature regions should be assigned respectively to the α_a relaxation processes in the internal phase and the interfacial layer.

However, there is a possibility that the sandwiched films were thermally damaged by the vacuum-deposition procedure [71], although such a damage was not visible in the microscopic observations. Hence, to investigate this likelihood, we prepared a PS1.46M ultrathin film sandwiched with SiO_x layers by laminating two PS films on SiO_x layers. In this case, the film should not have suffered any thermal damage. The result for the sandwiched film prepared by the lamination is also shown in Fig. 24 and clearly shows the additional peak in the higher temperature region. Although the intensity of the additional peak was different in the two sandwiched films prepared by different methods, their temperature regions seemed to be similar. Since the additional peak was observed only for the ultrathin PS film sandwiched with SiO_x layers, it is conceivable that the peak on the higher temperature side arose from an interfacial relaxation process and was not an experimental artifact.

Figure 25 shows the temperature dependence of relaxation time (τ_α) for the α_a relaxation processes in the internal and interfacial regions of the ultrathin PS1.46M film sandwiched between the SiO_x layers. Since it was hard to distinguish the temperature– τ_α relations between the vacuum deposited and laminated films, each data point was averaged over six independent measurements including both vacuum deposited and laminated films. The average thickness was about 40 nm. For comparison, the dashed curve in Fig. 25 denotes the bulk data obtained by the Vogel–Fulcher equation [72, 73]:

$$\tau_\alpha = \tau_0 \exp\left\{\frac{B}{T - T_v}\right\} \quad (14)$$

Here, T_v is the so-called Vogel temperature, at which the viscosity diverges to infinity. The parameter τ_0 is the characteristic time related to molecular vibration and B is the activation temperature. Even in the case of the internal phase, the

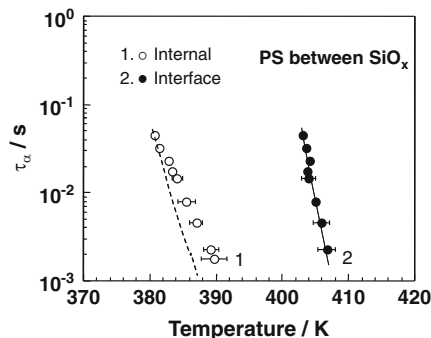


Fig. 25 Temperature dependence of τ_α for α_a relaxation processes in internal and interfacial regions of the PS1.46M ultrathin films sandwiched between SiO_x layers. The average thickness is about 40 nm. The *dashed curve* denotes the prediction of the Vogel–Fulcher equation using bulk parameters, whereas the *solid curve* is the best fit by Vogel–Fulcher equation for the interfacial α_a process

temperature dependence of τ_α slightly deviated from the bulk data. This discrepancy might be due to an effect of chain confinement, which appeared in the high molecular weight PS ultrathin films. However, Fig. 25 shows that the temperature relation in the interfacial layer was definitely different from that in the internal region. Since the interfacial α_a relaxation process seems to be independent of the internal relaxation process, the data set from the interfacial regions was fitted by the Vogel–Fulcher equation with a single Vogel temperature, as shown by the solid curve in Fig. 25. The T_v so obtained was 369 ± 4 K. Now, T_g is generally accepted to equal $(T_v + 50)$ K. So, even for this simplified case, the value of T_g in the interfacial layer should be 419 ± 4 K, a temperature higher than the T_g^b value of 378 K. This number is still averaged over a region with proximity to the substrate interface. Hence, the plausibility of this quantitative estimation for the interfacial T_g value merits further discussion. However, it is evident that the segmental mobility at the interface with the SiO_x layer is depressed in comparison with that for the bulk. This is in excellent accord with conclusions drawn from the previous section.

5 Conclusion

Thermal molecular motion of PS at surfaces and interfaces in films was presented in this review. We clearly show that chain mobility at the surface region is more mobile than in the interior bulk phase and that chain mobility at the interfacial region is less than in the interior phase. This means that there is a mobility gradient in polymer films along the direction normal to the surface. This gradient can be experimentally detected if the ratio of the surface and interfacial areas to the total volume increases, namely in ultrathin films.

Acknowledgments We deeply thank Professor Emeritus Tisato Kajiyama, Professor Emeritus Toshihiko Nagamura, Professor Daisuke Kawaguchi, Dr. Kei-ichi Akabori, and Dr. Yohei Tateishi for their fruitful discussion. This research was partly supported by Grant-in-Aid for Scientific Research (B) (No. 24350061), and for Science Research in a Priority Area “Soft Matter Physics” (No. 21015022) from the Ministry of Education, Culture, Sports, Science and Technology, Japan.

References

1. Stamm M (2008) Polymer surfaces and interfaces: characterization, modification and applications. Springer, Berlin
2. Karim A, Kumar S (2000) Polymer surfaces, interfaces and thin films. World Scientific, Singapore
3. Reiter G (1993) Europhys Lett 26:579
4. Keddie JL, Jones RAL, Cory RA (1994) Europhys Lett 27:59
5. Wallace WE, van Zanten JH, Wu WL (1995) Phys Rev E 52:R3329
6. DeMaggio GB, Frieze WE, Gidley DW, Zhu M, Hristov HA, Yee AF (1997) Phys Rev Lett 78:1524
7. Prucker O, Christian S, Bock H, Ruhe J, Frank CW, Knoll W (1998) Macromol Chem Phys 199:1435
8. Fryer DS, Nealey PF, de Pablo JJ (2000) Macromolecules 33:6439
9. See YK, Cha J, Chang T, Ree M (2000) Langmuir 16:2351
10. Kim JH, Jang J, Zin WC (2000) Langmuir 16:4064
11. Tsui OKC, Zhang HF (2001) Macromolecules 34:9139
12. Kim JH, Jang J, Zin WC (2001) Langmuir 17:2703
13. Kawana S, Jones RAL (2001) Phys Rev E 63:021501
14. Xie F, Zhang HF, Lee FK, Du B, Tsui OKC, Yokoe Y, Tanaka K, Takahara A, Kajiyama T, He T (2002) Macromolecules 35:1491
15. Forrest JA, Dalnoki-Veress K, Stevens JR, Dutcher JR (1996) Phys Rev Lett 77:2002
16. Forrest JA, Dalnoki-Veress K, Dutcher JR (1997) Phys Rev E 56:5705
17. Fukao K, Miyamoto Y (2000) Phys Rev E 61:1743
18. Ellison CJ, Torkelson JM (2003) Nat Mater 2:695
19. Inoue R, Kanaya T, Nishida K, Tsukushi I, Shibata K (2005) Phys Rev Lett 95:056102
20. Miyazaki T, Nishida K, Kanaya T (2004) Phys Rev E 69:061803
21. O’Connell PA, McKenna GB (2005) Science 307:1760
22. Kajiyama T, Tanaka K, Ohki I, Ge SR, Yoon JS, Takahara A (1994) Macromolecules 27:7932
23. Tanaka K, Hashimoto K, Takahara A, Kajiyama T (2003) Langmuir 19:6573
24. Kajiyama T, Tanaka K, Takahara A (1997) Macromolecules 30:280
25. Hammerschmidt JA, Gladfelter WL, Haugstad G (1999) Macromolecules 32:3360
26. Tanaka K, Takahara A, Kajiyama T (2000) Macromolecules 33:7588
27. Akabori K, Tanaka K, Kajiyama T, Takahara A (2003) Macromolecules 36:4937
28. Mayes AM (1994) Macromolecules 27:3114
29. Tanaka K, Taura A, Ge SR, Takahara A, Kajiyama T (1996) Macromolecules 29:3040
30. Tanaka K, Takahara A, Kajiyama T (1997) Macromolecules 30:6626
31. Kajiyama T, Tanaka K, Satomi N, Takahara A (1998) Macromolecules 31:5150
32. Tanaka K, Jiang X, Nakamura K, Takahara A, Kajiyama T, Ishizone T, Hirao A, Nakahama S (1998) Macromolecules 31:5148
33. Satomi N, Takahara A, Kajiyama T (1999) Macromolecules 32:4474
34. Kajiyama T, Satomi N, Yokoe Y, Kawaguchi D, Tanaka K, Takahara A (2000) Macromol Symp 159:35
35. Ferry JD (1980) Viscoelastic properties of polymers, 3rd edn. Wiley, New York

36. Bueche F (1955) *J Appl Phys* 26:738
37. Takayanagi M (1965) In: Lee EH, Copley AL (eds) *Proceedings of the 4th international congress on rheology, part 1*, Brown University, Providence, 26–30 August 1963. Butterworth, London, pp 161–187
38. McCrum NG, Read BE, Williams G (1967) *Anelastic and dielectric effects in polymeric solids*. Dover, New York
39. Santangelo PG, Roland CM (1998) *Macromolecules* 31:4581
40. Kawaguchi D, Tanaka K, Kajiyama T, Takahara A, Tasaki S (2003) *Macromolecules* 36:1235
41. Kremer K, Grest GS (1990) *J Chem Phys* 92:5057
42. Morita H, Tanaka K, Kajiyama T, Nishi T, Doi M (2006) *Macromolecules* 39:6233
43. Krishnamoorti R, Vaia RA (eds) (2001) *Polymer nanocomposites: synthesis, characterization, and modeling*. In: ACS Symposium Series, vol 804. American Chemical Society, Washington
44. Ray SS, Bousmina M (2006) *Polymer nanocomposites and their applications*. American Scientific, Stevenson Ranch
45. Mai YW, Yu ZZ (2006) *Polymer nanocomposites*. CRC, Boca Raton
46. Shchipunov YA, Karpenko TY (2004) *Langmuir* 20:3882
47. Bordes P, Pollet E, Bourbigot S, Averous L (2008) *Macromol Chem Phys* 209:1473
48. Godovsky DY (2000) *Adv Polym Sci* 153:163
49. Tao SY, Yin JX, Li GT (2008) *J Mater Chem* 18:4872
50. Harmer MA, Farneth WE, Sun Q (1996) *J Am Chem Soc* 118:7708
51. Hasani-Sadrabadi MM, Emami SH, Moaddel H (2008) *J Power Sources* 183:551
52. Kim GM, Lee DH, Hoffmann B, Kressler J, Stoppelmann G (2001) *Polymer* 42:1095
53. Tien YI, Wei KH (2001) *Macromolecules* 34:9045
54. Tanaka K, Tsuchimura Y, Akabori K, Ito F, Nagamura T (2006) *Appl Phys Lett* 89:061916
55. Tanaka K, Tateishi Y, Okada Y, Nagamura T, Doi M, Morita H (2009) *J Phys Chem B* 113:4571
56. Matsuoka H (2001) *Macromol Rapid Commun* 22:51
57. Owens DK, Wendt RC (1969) *J Appl Polym Sci* 13:1741
58. Knoll W (1998) *Annu Rev Phys Chem* 49:569
59. Ekgasit S, Thammacharoen C, Knoll W (2004) *Anal Chem* 76:561
60. Tsuruta H, Fujii Y, Kai N, Kataoka H, Ishizone T, Doi M, Morita H, Tanaka K (2012) *Macromolecules* 45:4643.
61. Alcoutlabi M, McKenna GB (2005) *J Phys Condens Matter* 17:R461
62. Baschnagel J, Varnik F (2005) *J Phys Condens Matter* 17:R851
63. Forrest JA, Dalnoki-Veress K (2001) *Adv Coll Interf Sci* 94:167
64. Roth CB, Dutcher JR (2005) *J Electroanal Chem* 584:13
65. Tsui OKC, Russel TP (2008) *Polymer thin films. Series in soft condensed matter*. World Scientific, Singapore
66. Keddie JL, Jones RAL, Cory RA (1994) *Faraday Discuss* 98:219
67. van Zanten JH, Wallace WE, Wu WL (1996) *Phys Rev E* 53:R2053
68. Reiter G (1994) *Macromolecules* 27:3046
69. Tsui OKC, Russell TP, Hawker C (2001) *Macromolecules* 34:5535
70. Takayanagi M, Imada K, Kajiyama T (1967) *J Polym Sci C* 15:263
71. Yan S (2003) *Macromolecules* 36:339
72. Vogel H (1921) *Phys Z* 22:645
73. Fulcher GS (1925) *J Am Ceram Soc* 77:3701